SECURITY CLASSIFICATION OF THIS PAGE *(When Data Entered)*

REPORT DOCUMENTATION PAGE	READ INSTRUCTIONS BEFORE COMPLETING FORM

1. REPORT NUMBER	2. GOVT ACCESSION NO.	3. RECIPIENT'S CATALOG NUMBER
Technical Report BRL-TR-2662		

4. TITLE *(and Subtitle)*	5. TYPE OF REPORT & PERIOD COVERED
MODELING ADIABATIC SHEAR	Final
	6. PERFORMING ORG. REPORT NUMBER

7. AUTHOR(s)	8. CONTRACT OR GRANT NUMBER(s)
Barbara E. Ringers	

9. PERFORMING ORGANIZATION NAME AND ADDRESS	10. PROGRAM ELEMENT, PROJECT, TASK AREA & WORK UNIT NUMBERS
US Army Ballistic Research Laboratory ATTN: AMXBR-TBD Aberdeen Proving Ground, MD 21005-5066	RDTE 1L162618AH80

11. CONTROLLING OFFICE NAME AND ADDRESS	12. REPORT DATE
US Army Ballistic Research Laboratory ATTN: AMXBR-OD-ST Aberdeen Proving Ground, MD 21005-5066	July 1985
	13. NUMBER OF PAGES
	40

14. MONITORING AGENCY NAME & ADDRESS*(if different from Controlling Office)*	15. SECURITY CLASS. *(of this report)*
	UNCLASSIFIED
	15a. DECLASSIFICATION/DOWNGRADING SCHEDULE

16. DISTRIBUTION STATEMENT *(of this Report)*

Approved for public release; distribution unlimited.

17. DISTRIBUTION STATEMENT *(of the abstract entered in Block 20, if different from Report)*

18. SUPPLEMENTARY NOTES

19. KEY WORDS *(Continue on reverse side if necessary and identify by block number)*

Terminal Ballistics	EPIC-2
Lagrangian	Adiabatic Shear
Kinetic Energy	
Simulation	
Plugging	

20. ABSTRACT *(Continue on reverse side if necessary and identify by block number)*

This paper discusses the techniques and criteria developed to simulate target plugging failure due to adiabatic shear and presents simulations of two impacts involving steel rods against titanium alloy targets. A Lagrangian dynamic impact code, EPIC-2, was utilized as the basis for this effort. A stress/(strain, strain rate, temperature) relationship in which temperature was based on the conversion of plastic work into heat, was utilized for the target material; newly developed sliding surface

DD ¹ FORM 73 **1473** EDITION OF 1 NOV 65 IS OBSOLETE

techniques combined with an adiabatic slip criterion controlled target failure. Results indicate that such techniques show considerable promise in modeling this complex phenomenon.

0142

US ARMY
MATERIEL
COMMAND

AD

TECHNICAL REPORT BRL-TR-2662

MODELING ADIABATIC SHEAR

Barbara E. Ringers

July 1985

US ARMY BALLISTIC RESEARCH LABORATORY
ABERDEEN PROVING GROUND, MARYLAND

TABLE OF CONTENTS

3

LIST OF ILLUSTRATIONS

5

List of Illustrations

I. INTRODUCTION

Plugging due to adiabatic shear is a prevalent mode of target failure in both rolled homogeneous armor targets and high hard armor targets. It is therefore of considerable terminal ballistic interest to be able to accurately model this phenomenon. This paper presents techniques and criteria developed to handle simulations of target plugging failure due to adiabatic shear and compares experiment and simulations for two impacts involving titanium alloy targets.

II. SLIDING SURFACE TECHNIQUES

A Lagrangian, dynamic impact code, EPIC-2,[1] was utilized as the basis for this effort. Major modifications had been developed and implemented by the author to provide the mechanics necessary to handle deep penetration/ perforation of targets.[2] Splitting between target elements (triangles in EPIC-2) was utilized to simulate shearing failure (Figure 1) and total element failure was enabled to simulate the expected accompanying erosion in both projectile and target. An automatic dynamic relocation of sliding surfaces including the addition of new sliding surfaces, when appropriate, enabled both of these target failure techniques to carry a calculation to completion, i.e., through target perforation, if applicable. The beauty of these sliding surface techniques is that they provide the mechanics by which criteria may be tested for their capabilities in handling specific modes of target failure. These techniques were first successfully applied in conjunction with an equivalent strain criterion to handle the modeling of plugging failure due to high strains.[3]

III. APPROACH TO MODELING ADIABATIC SHEAR

A. Constitutive Equations

Prior to enabling splitting between elements, the impact of a steel cylinder against a Ti318 (6%Al, 4%V) target at a striking velocity of 455 m/s

----

1. Johnson, Gordon R., "EPIC-2, A Computer Program for Elastic-Plastic Impact Computations in 2 Dimensions Plus Spin," US Army BRL Contract Report ARBRL-CR-00373, June, 1978. (AD A058 786)
2. Ringers, B. E., "New Sliding Surface Techniques Enable Lagrangian Code to Handle Deep Target Penetration/Perforation Problems," Computational Aspects of Penetration Mechanics, Lecture Notes in Engineering, Springer-Verlag, 1983.
3. Ringers, B. E., "Simulations of Ballistic Impact Situations Involving Deep Penetration and Perforation of Targets With a Lagrangian Impact Code," Proceedings of the Army Symposium on Solid Mechanics, 1982 - Critical Mechanics Problems in Systems Design, AMMRC MS 82-4, September 1982.

Figure 1.   Splitting Between Elements.

TI 318 TARGET

Z AXIS (m x 10⁻¹)

R AXIS (m x 10⁻¹)

NO SIGN OF SHEAR BAND
BY 10 μs

TI 125 TARGET

Z AXIS (m x 10⁻¹)

R AXIS (m x 10⁻¹)

INCIPIENT SHEAR BAND
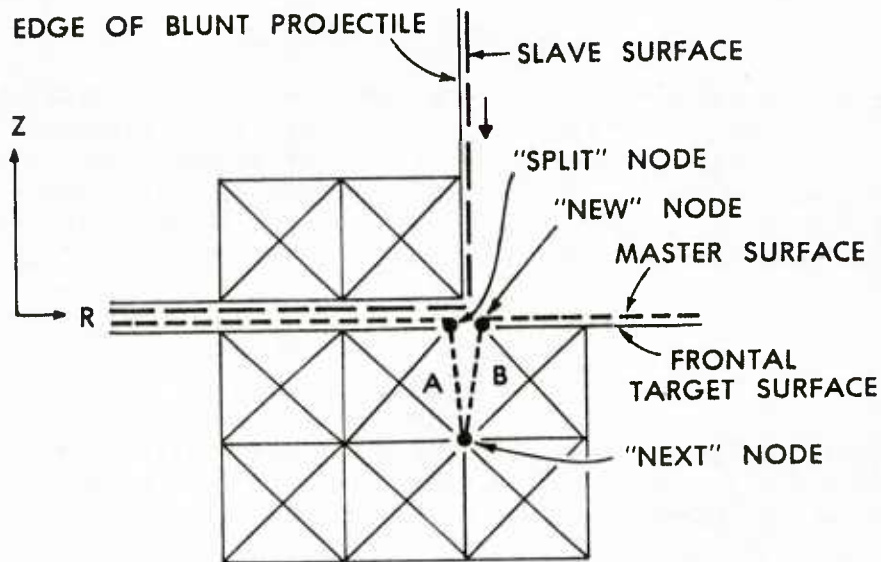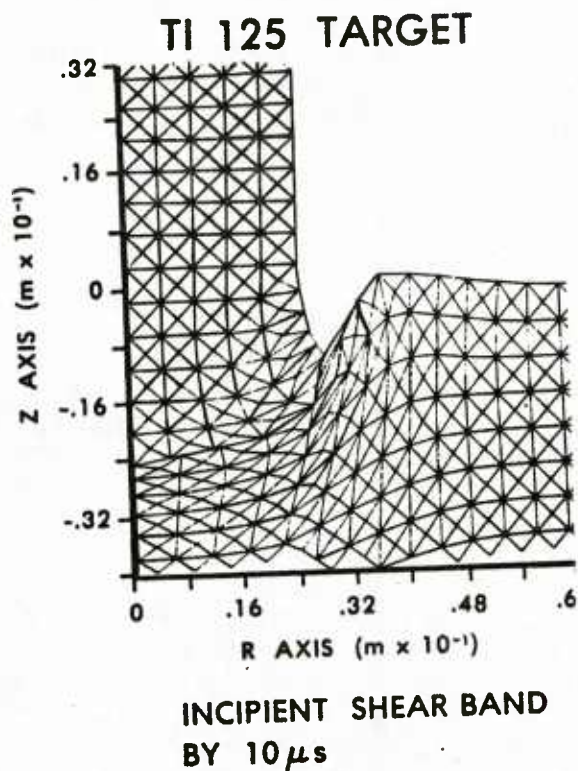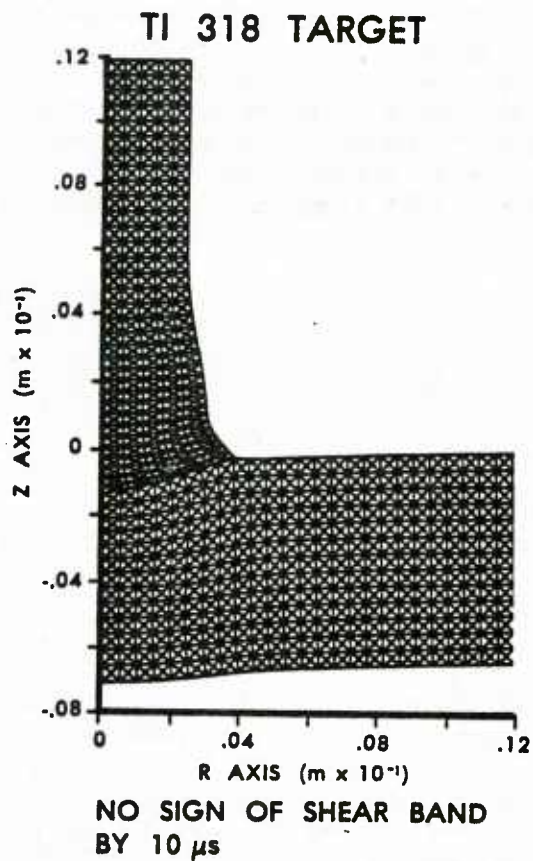BY 10 μs

Figure 2.   Impact of Steel Cylinder vs
Ti 318 Target at 455 m/s No Splitting
Enabled.

Figure 3.   Impact of Steel Cylinder vs
Ti 125 Target at 350 m/s No Splitting
Enabled.

was simulated (Figure 2). The Ti318 material is known to fail by adiabatic shear. Contrast these results with those for the impact of a similar steel cylinder against a Ti125 (99% pure Ti) target at 350 m/s (Figure 3). Although the first case involved a much higher striking velocity, there is no sign of an incipient shear band by 10×10^{-6} s whereas in the second case plugging failure is due to high strains and an incipient shear band is demonstrated. Such diverse results, and indeed an attempt with the same simulation techniques, indicated that adiabatic shear can not be successfully modeled utilizing only a linear elastic/plastic stress/strain relationship and an equivalent strain criterion, the combination which was successful in modeling plugging due to high strains for the Ti125 target. Ti318 has a considerably lower work hardening rate, a much higher yield strength, and a higher thermal softening rate than Ti125 as evidenced by material tests conducted by Wulf.[4]

Recht[5] demonstrated that low values of thermal conductivity, density, specific heat, and work hardening rate and high values of thermal softening rate and yield strength were conducive to adiabatic shear. The author's plan was to take into consideration the temperature rise due to the conversion of plastic deformation into heat.

Johnson[6] suggested expressing stress as the following analytic function of strain, strain rate and temperature for the Ti318 target material:

$$\sigma = (A + B \, \epsilon^n) \, (1 + C \ln (\dot{\epsilon}/\dot{\epsilon}_o) \, K_T$$

where A, B, n, and C are material parameters,

$$K_T = 1 - (T - T_R)/(T_M - T_R)$$

and T, T_R, and T_M are present, room, and melting temperature respectively. Johnson had utilized this form for the shear stress and had reasonable agreement with actual test data for several materials.[7]

The first expression is an isothermal relationship between stress and strain. Lindholm[8] had demonstrated that a logarithmic relationship between stress and rate held over a range of strain rates from 10^{-4} s^{-1} to 10^3 s^{-1};

---

4. Wulf, G. L., "High Strain Rate Compression of Titanium and Some Titanium Alloys," Int. J. Mech. Sci., Vol. 21, 1979.
5. Recht, R. F., "Catastrophic Thermoplastic Shear," Journal of Applied Mechanics, June, 1964, pp. 189-193.
6. Johnson, Gordon R., Private Communication.
7. Johnson, G. R., Hoegfeldt, J. M., Lindholm, U. S., and Nagy, A., "Response of Various Metals to Large Torsional Strains Over A Large Range of Strain Rates - Part 2; Less Ductile Metals," Journal of Engineering Materials and Technology, January, 1983, p. 48.
8. Lindholm, U.S., "Some Experiments with the Split Hopkinson Pressure Bar," J. Mech. Phys. Solids, Vol. 12, 1964, p. 317.

hence, the second expression. K_T is a linear thermal softening expression and varies from $K_T = 1$ at room temperature to $K_T = 0$ at melting temperature.

The author utilized data for titanium (6%Al, 4%V) published by Maiden and Green.[9] Specifically, curve fitting techniques were applied to the stress/strain curve for $\dot{\epsilon} = 1.5$ s^{-1} $\approx$ $\dot{\epsilon} = 1$ s^{-1} to determine the best values for A, B, and n assuming $\dot{\epsilon}_0 = 1$ s^{-1}. C was then calculated applying the values of A, B, and n to the curve for $\dot{\epsilon} = 20$ s^{-1}. It was assumed that thermal effects were not involved at such low strain rates; therefore $K_T = 1$ for these determinations.

The values of material parameters A, B, n, and C (0., 1896.2, .095, .0226, respectively) and the melting temperature (1660° C) became user input parameters to this highly modified EPIC-2 code. For an individual target element, strength as a function of strain, strain rate and temperature was utilized only after the yield strength (1029 MPa) was reached, thereby retaining a linear elastic relationship.

The adiabatic temperature rise is given by:

$$\Delta T = \frac{1}{\rho \bar{C}_p} \int_o^\gamma \tau \, d\gamma \qquad (10)$$

where ρ = density,

$\bar{C}_p$ = mean specific heat

τ = stress when the plastic strain is γ.

The author assumed constant stress for the increment of time involved and utilized a product of equivalent stress ($\bar{\sigma}$), equivalent strain rate ($\dot{\bar{\epsilon}}$) and the current time increment for the power input.

Since estimates vary from 85% to almost 100% as to what proportion of the work of plastic deformation is converted into heat[11, 12, 13] calculations utilizing both of these limits were performed.

----

9. Maiden, C. J., Green, S. J., "Compressive Strain-Rate Tests on Six Selected Materials at Strain Rates From 10^{-3} to 10^4 In/In/Sec," Transactions of the ASME, September, 1966, p. 496.
10. Campbell, J. D. and Ferguson, W. G., "The Temperature and Strain-Rate Dependence of the Shear Strength of Mild Steel," Phil. Mag., Vol. 21, 1970, p. 63.
11. Johnson, W., Impact Strength of Materials, Edward Arnold Ltd., 1972.
12. Rogers, Harry C., "Adiabatic Plastic Deformation," Ann. Rev. Mater. Sci., Vol. 9, 1979, p. 283.
13. Titchener, A. L. and Bever, M. B., Progr. Metal Phys., Vol. 7, 1958.

B. Development of Criteria Mandating Target Failure

"If the rate of decrease in strength, resulting from the local increase in temperature, equals or exceeds the rate of increase in strength, due to the effects of strain-hardening, the material will continue to deform locally. This unstable process leads to the catastrophic condition known as adiabatic slip." - Recht.[5]

Webster defines "adiabatic" as occurring without loss or gain of heat. Rogers[12] notes that although the term "adiabatic" is misleading since heat is lost to the surroundings at a rapid rate, the heat loss is small relative to heat generation. The velocities involved in typical ballistic impacts result in strain rates of $10^5 - 10^6$ s^{-1} and the period of time (microseconds) means there is insufficient time for the heat generated by such strain rates to be dissipated by conduction; hence, adiabatic slip or shear.

This, then, is the basis for the most important criterion in attempting to model adiabatic shear - when the rate of thermal softening overcomes the rate of strain hardening, i.e., when $\partial\sigma/\partial\epsilon = 0$.

The following criteria were developed and utilized to simulate the adiabatic shear responsible for plugging failure:

Criterion 1: An element initiates or furthers a split
1) when the rate of thermal softening > rate of work hardening, and
2) when, if furthering a split, it is associated with the "next" node, and
3) when the magnitude of its shear stress > the magnitudes of its deviatoric axial and radial stresses, and
4) when the direction of the split (Criterion 3) is not to a node with a higher z coordinate.

Criterion 2: The node at which initial splitting occurs
1) must belong to the element meeting Criterion 1,
2) must suffer the highest force of all three nodes belonging to the same element, and
3) must be a master node.

Criterion 3: The direction of the split is determined by the strain of the element meeting Criterion 1. In general, if the magnitude of the axial strain > the magnitude of the radial strain, splitting is to the nearer radial node. Otherwise, splitting is to the node closer to the direction of radial strain.

IV. CASE I

A. Experimental Results

Woodward fired five shots of hardened, roller-bearing steel cylinders

11

into Ti318 targets at normal obliquity.[14]   Note the geometric and material
properties for the first penetrator and target, Table 1. The minimum velocity
at which target perforation occurred was 441 + 14 m/s. In every case the
projectile fractured. In one case plugging due to adiabatic shear occurred;
the plug was pushed through the target but a small part of the projectile
stayed in the target while the remainder rebounded (Figure 4a). However the
adiabatic shear band was so narrow that it took metallographic analysis (1000X
magnification) to ascertain that it definitely was adiabatic shear. In two
other cases the projectile broke up and ricocheted and the plug was not
pushed out; the shear band did not reach the rear surface of the target but
did precede the crack (Figure 4b).

B. Simulations and Comparisons

The calculations to simulate this situation utilized a striking velocity
of 455 m/s. An axisymmetric deformation history of the calculation when 100%
plastic work was assumed converted to heat is shown in Figure 5. Axisymmetric
blowups of the region of activity for the simulations assuming 100% and 85%
conversions, respectively, are shown in Figures 6a and 6b. The corresponding
patterns of elements which enabled splitting and the elements which totally
failed are shown in Figures 7a and 7b. Note that when 100% plastic work was
assumed converted to heat, the shear band reached the rear target surface at
3.25×10^{-6} s implying a crack velocity of 1954 m/s. (The sound speed of
Ti318 $\simeq$ 1966 m/s.) The plug was completely formed and was pushed
approximately 1.5 mm past the rear target surface. The forward motion of the
projectile stopped between 25×10^{-6} s and 30×10^{-6} s and the projectile is
progressively rebounding at 30×10^{-6} s and 35×10^{-6} s. Note that several
projectile and target elements were automatically totally failed, primarily
on the basis of a minimum time increment violation. (See Appendixes A and B
for specifics on element failure.) There were some problems with overlap of
elements on the same sliding surface with so much element failure; surface
elements can not interfere with elements on another surface but there is no
provision for checking interference between elements on the same surface.
The speed histories of the projectile are shown in Figure 8, the
depth-of-penetration histories in Figure 9.

Distinctions between the results of simulations using 100% and 85%
conversion of plastic work into heat, respectively, are almost negligible.
In general, the shear band developed a little more slowly and rebound
occurred a little later for 85% conversion; the crack velocity was 1890 m/s.
The results of the calculations are promising when compared with the
experimental evidence with regard to the shape of the deformed rod, the
total failure of part of the projectile, the formation of the plug, even the
inward-directed angle toward the bottom of the incompletely-formed plug when
the velocity is just under the limit velocity. However, the crack velocities
would seem to be unreasonably close to the sound speed of the material and

----

14. Woodward, R. L., Private Communication - experiments performed at
Materials Research Laboratories, Australia.

MATERIAL	PENETRATOR 1 STEEL	TARGET 1 Ti 318 (Ti WITH 6% Al, 4%V)	PENETRATOR 2 STEEL	TARGET 2 Ti 318 (Ti WITH 6% Al, 4% V)
SHAPE	BLUNT	50 mm SQUARE	BLUNT	50 mm SQUARE
MASS	3.34 g	—	3.34 g	—
LENGTH	25.4 mm	THICK *6.35mm*	25.4 mm	THICK *6mm*
DIAMETER	4.76 mm	—	4.76 mm	—
DENSITY	$7.39 \times 10^3 kg/m^3$	$4.43 \times 10^3 kg/m^3$	$7.39 \times 10^3 kg/m^3$	$4.43 \times 10^3 kg/m^3$
σ_Y	*2290 MPa*	1029 MPa	*2233 MPa*	1029 MPa
σ_U	2500 MPa	1209 MPa	2500 MPa	1209 MPa
ϵ_U	—	0.2	—	0.2
SPECIFIC HEAT	—	$5.65 \times 10^2 J/kg\,°C$	—	$5.65 \times 10^2 J/kg\,°C$
YOUNGS MOD	$1.93 \times 10^5 MPa$	$1.158 \times 10^5 MPa$	$1.93 \times 10^5 MPa$	$1.158 \times 10^5 MPa$

Table 1. Geometric and Material Properties Case I and II.

PROJECTILE PIECE REBOUNDED

PROJECTILE PIECE STUCK IN TARGET

PLUG PUSHED OUT

PLUGGING, PERFORATION

SHEAR BAND
CRACK

INCIPIENT PLUGGING & PROJECTILE REBOUND
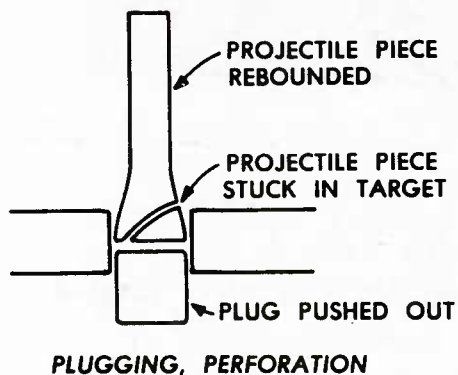
Figure 4a. Sketch of Experimental Results - Case I - Woodward.

Figure 4b. Sketch of Incipient Plugging $V_S < V_L$ - Woodward.

STEEL CYLINDER vs TI 318 TARGET

0 µs

5 µs

20 µs

35 µs
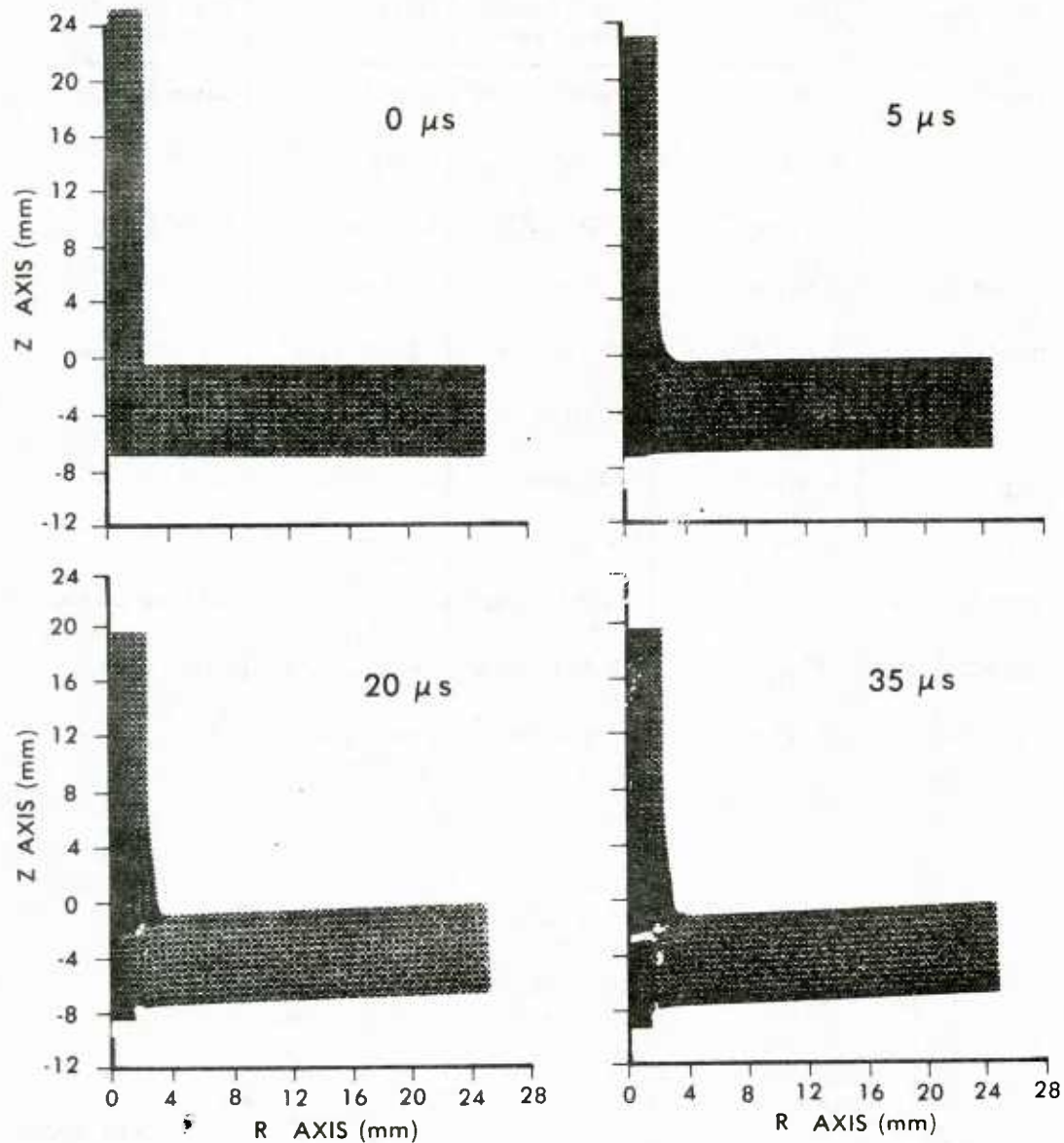
V_S = 455 m/s

σ_Y(PENETRATOR) = 2290 MPa

TARGET THICKNESS = 6.35 mm

PERFORATION @ 3.25 µs
REBOUND OF PENETRATOR
BETWEEN 25 & 30 µs

Figure 5. Deformation History - Case I,
100% Plastic Work Converted to Heat.

14
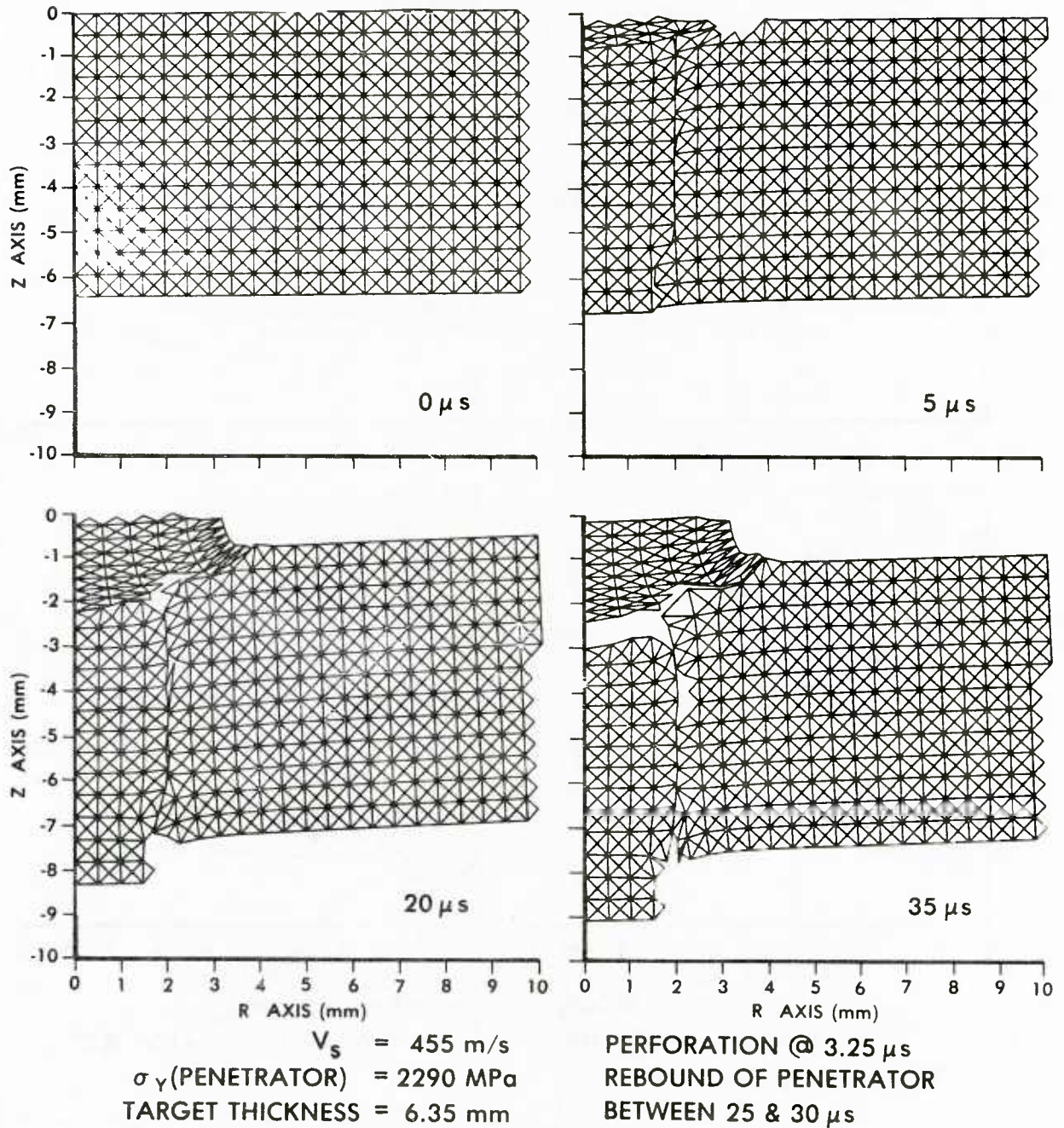
Figure 6a.   Axisymmetric Blowup of Region of Activity - Case I.
100% Plastic Work Converted to Heat.

15

STEEL CYLINDER vs TI 318 TARGET
BLOW UP OF REGION OF ACTIVITY
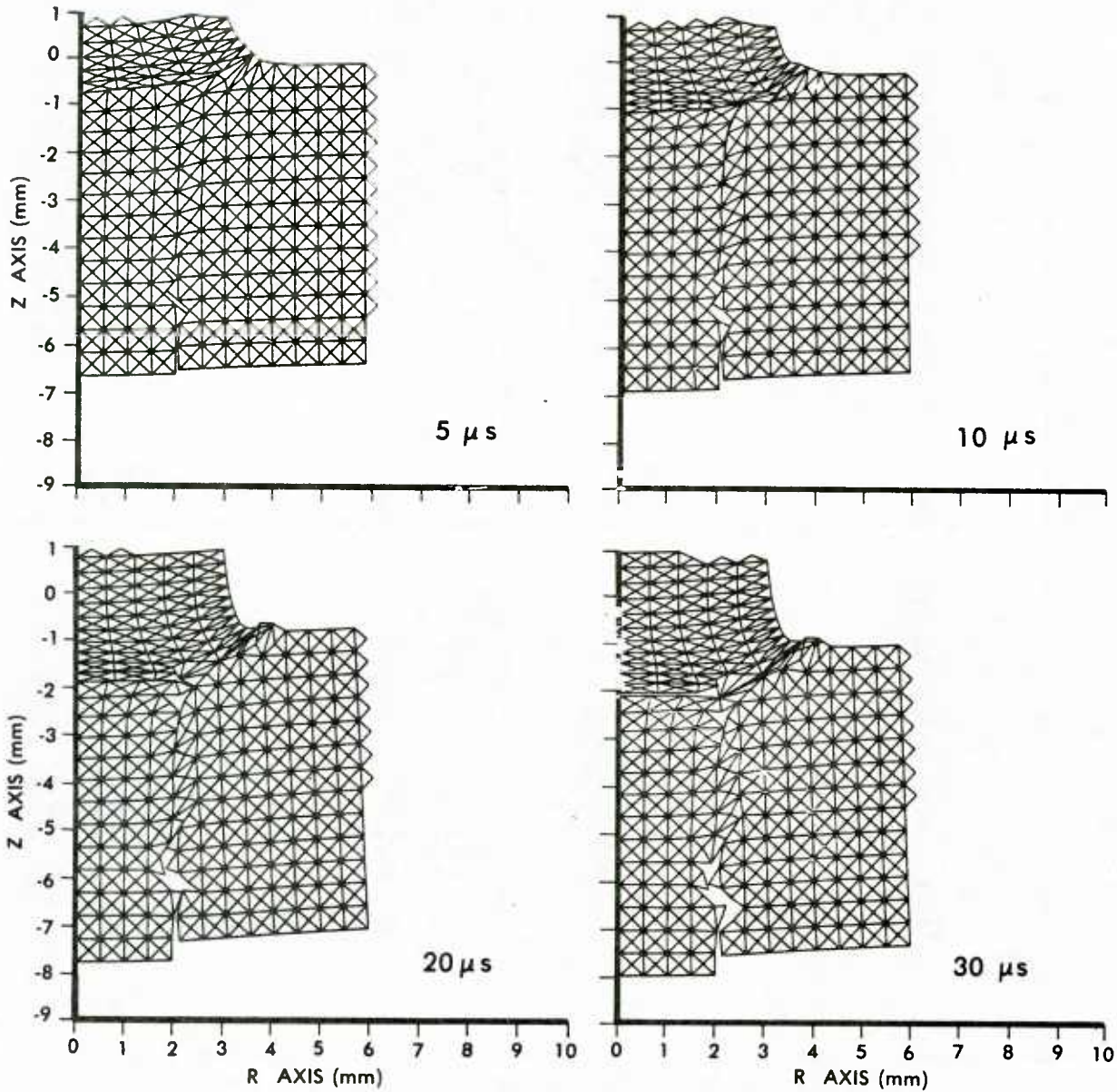
V_s = 455 m/s

σ_Y(PENETRATOR) = 2290 MPa

TARGET THICKNESS = 6.35 mm

PERFORATION @ 3.36 μs

REBOUND OF PENETRATOR @ 25 μs

Figure 6b. Axisymmetric Blowup of Region of Activity - Case I.
85% Plastic Work Converted to Heat.

Figure 7a. Pattern of Elements Enabling
Split - Case I.   100% Plastic Work
Converted to Heat.

Figure 7b. Pattern of Elements Enabling
Split - Case I.   85% Plastic Work Converted
to Heat.

Figure 8. Speed Histories - Case I.

Figure 9. Depth of Penetration Histories - Case I.
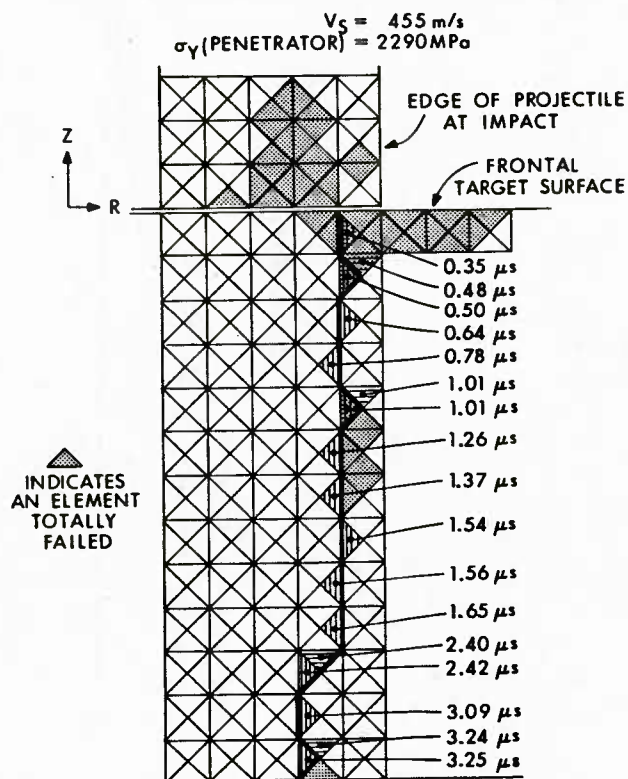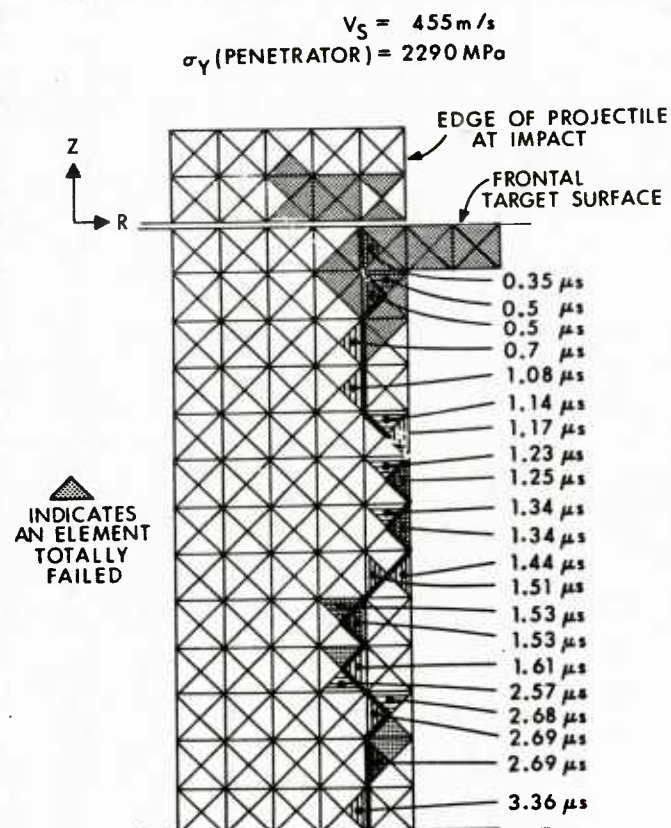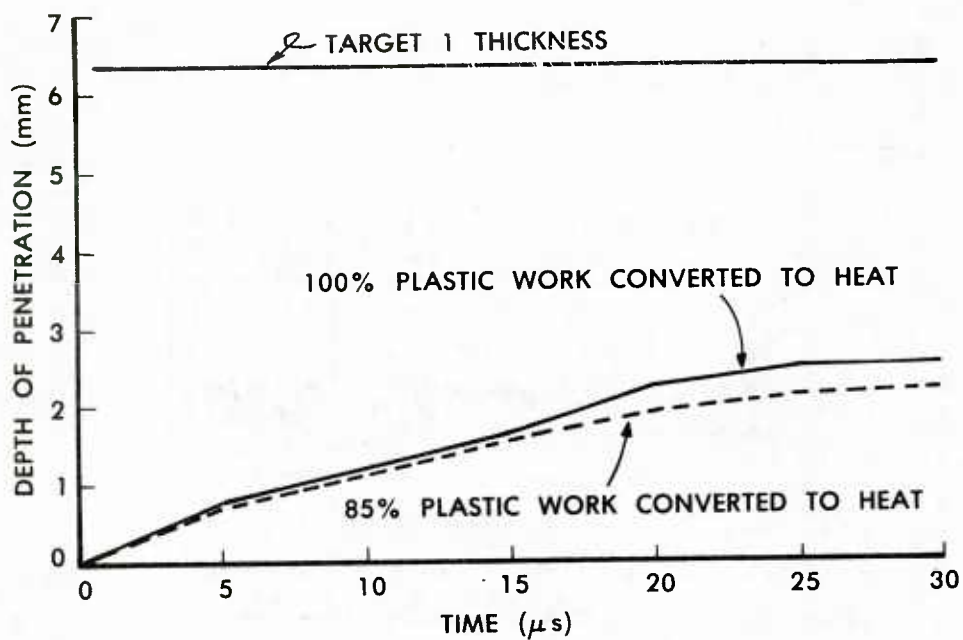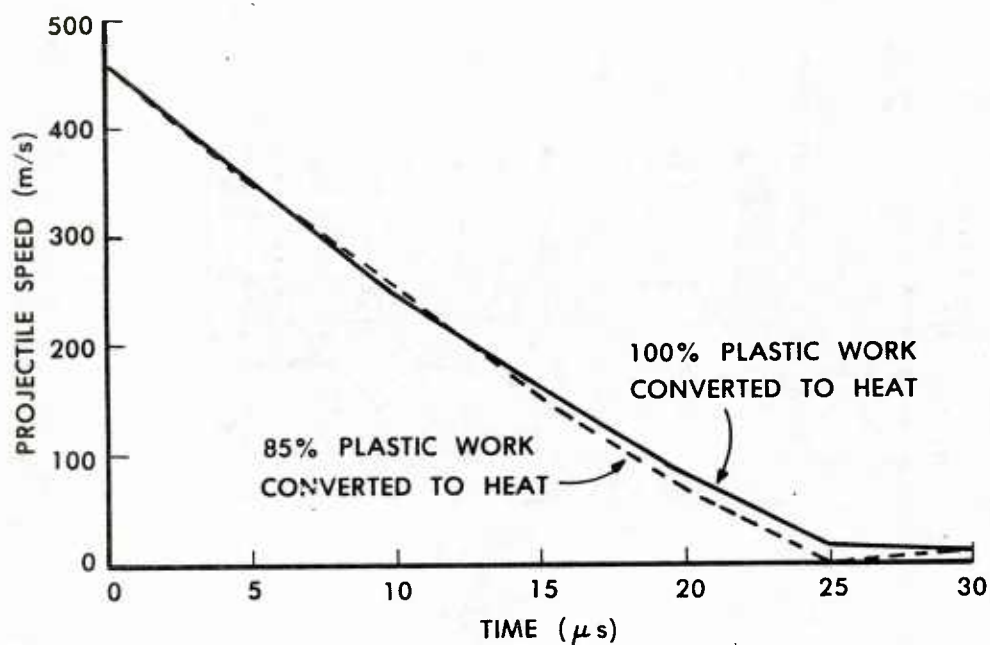
18

the jaggedness of the splitting pattern detracts from the results of the simulation. A calculation was made utilizing the stress/(strain, strain rate, temperature) relationship with splitting disabled; the instability worked its way down through a "bandwidth" of elements; it was not as localized as might be expected.

Of more concern, perhaps, is the placement of the split, not directly under the edge of the projectile. This is the result of a built-in bias in the method. The forces on a node are based on the stresses of the elements sharing that node. The forces on a node under the edge of the projectile will depend upon the high stresses of the elements under the projectile as well as the lower stresses of the elements outside the projectile periphery whereas the forces on an inner node will be based on the stresses of elements, all of which are directly under the impact. The nodal accelerations calculated for these inner nodes will be higher and will similarly affect the nodal velocities and, in turn, the element strain rates, strains, and stresses. Therefore the elements vertically aligned close to, but not directly under, the edge of the projectile will attain prescribed failure criteria earlier than those aligned with the edge. This bias and the jagged splitting pattern would, of course, not be as noticeable if the grid resolution was much finer.

V. CASE II

A. Experimental Results

The second case for which simulations were calculated was experimental work only recently conducted by Woodward, Baxter, and Scarlett.[15] A blunt steel cylinder with corners ground to a radius of .25 mm impacted a Ti318 target at normal obliquity with a striking velocity of 247 m/s. Results (Figure 10) indicate very little plug compression and the separation of a plug from the remaining target material at several places, but not everywhere, along the band. Woodward, et al., noted that examinations of sections parallel to the plane of the plate showed the separate nucleation of very narrow shear bands and their independent propagation to the rear surface despite joining circumferentially in several positions. They also noted an initial acceleration phase during which compression takes place preceding the formation of the adiabatic shear band.

This case differed from the first case in the significantly lower striking velocity (247 m/s vs 455 m/s), the lower hardness of the projectile (2233 MPa vs 2290 MPa), and the different target thickness (6 mm vs 6.35 mm).

B. Simulations and Comparisons

These simulations utilized a striking velocity of 247 m/s and the

----

15. Woodward, R. L., Baxter, B. J. and Scarlett, N. V. Y., "Mechanisms of Adiabatic Shear Plugging Failure in High Strength Aluminum and Titanium Alloys," 3rd International Conference on Mechanical Properties of Materials At High Rates of Strain," Oxford, April, 1984.
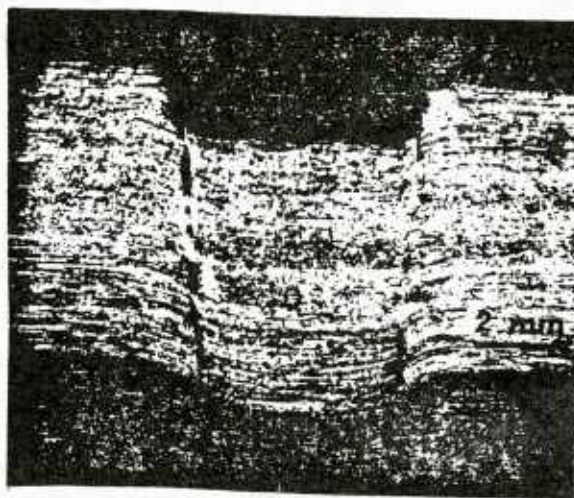
Figure 10.   Section of Ti 318
          - Case II. (15)

geometric and material properties noted for the second penetrator and target in Table 1. The axisymmetric deformation history for 100% conversion of plastic work to heat is shown in Figure 11; blowups of the region of activity are shown in Figures 12a and 12b for the 100% and 85% conversions, respectively. Very jagged splitting patterns are evident for the simulations in Figure 13. Only two projectile elements were totally failed due to a minimum time increment violation before projectile rebound occurred for the 100% conversion simulation. The shear band in this case did not reach the rear target surface until 8.28×10^{-6} s, implying a crack velocity of 725 m/s. A plug was completely formed and extends slightly ($\approx$.3 mm) from the rear of the target. There was no discernible plug compression; the projectile began to rebound by 20×10^{-6} s. The speed and depth-of-penetration histories for both simulations are shown in Figures 14 and 15. Again the simulation performed with 85% plastic work converted to heat produced similar results. Note, however, that although the speed and depth of penetration histories are similar for the 100% and 85% conversions for both calculations there is one noticeable difference. Whereas at a striking velocity of 455 m/s the 100% conversion of plastic work to heat generally resulted in a slightly higher velocity and slightly greater depth of penetration than with 85% conversion during penetration, at 247 m/s, a little less than the minimum velocity for perforation, the results would seem to be the reverse of this. Splitting, in general, proceeded a little faster with 100% conversion until the last couple of layers but rebound also started to occur earlier limiting the depth of penetration more but rebounding at a slightly higher speed (4.48 m/s for 100% conversion vs 3 m/s for 85% conversion).

Comparison between the more detailed experimental results in this case and the simulations is most interesting - the correspondingly slower formation of a plug which was not ejected, the highly jagged pattern in the simulation coincidentally reflecting the areas of separation and nonseparation (due possibly to subsequent welding) of plug from the remaining target.

Again the placement of the split is biased toward the axis. The small, but discernible, compression of the plug and the significant indentation of the target in the experiment was not matched in the simulations. It was thought that if the simulation was allowed a longer plug acceleration period before splitting was enabled, target compression might result (as occurred with the Ti125 target in Figure 3). However, the calculation performed with splitting disabled indicated no noticeable compression of the target elements by 10×10^{-6} s.

VI. CONCLUSIONS

This paper presented simulations of target plugging failure due to adiabatic shear utilizing finite element techniques, a stress/(strain, strain rate, temperature) relationship, and the monitoring of the instability which occurs when thermal softening overwhelms work hardening. Simulations and comparisons with two experiments indicate considerable promise for the method; plugging was correctly predicted in the simulations and results were consistent between calculations - a much higher striking velocity producing

STEEL CYLINDER vs TI 318 TARGET
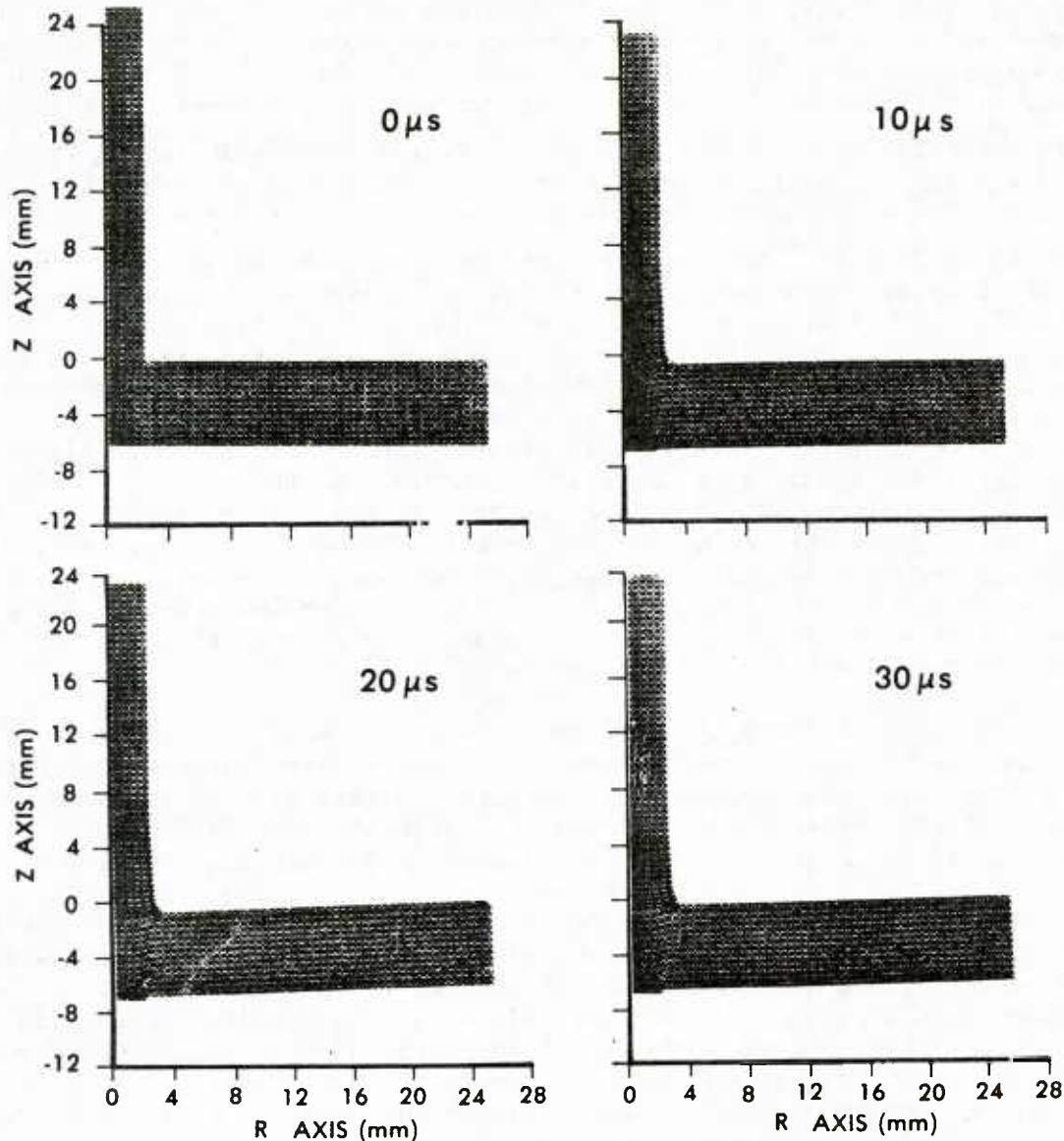
$V_S = 247$ m/s

σ_Y (PENETRATOR) $= 2233$ MPa

TARGET THICKNESS $= 6$ mm

PERFORATION @ $8.28\,\mu$s

REBOUND OF PENETRATOR @ $< 20\,\mu$s

Figure 11. Deformation History - Case II.
100% Plastic Work Converted to Heat.

22

STEEL CYLINDER vs TI 318 TARGET
BLOW UP OF REGION OF ACTIVITY

V_s = 247 m/s

σ_Y (PENETRATOR) = 2233 MPa

TARGET THICKNESS = 6 mm

PERFORATION @ 8.28 μs

REBOUND OF PENETRATOR @ < 20 μs
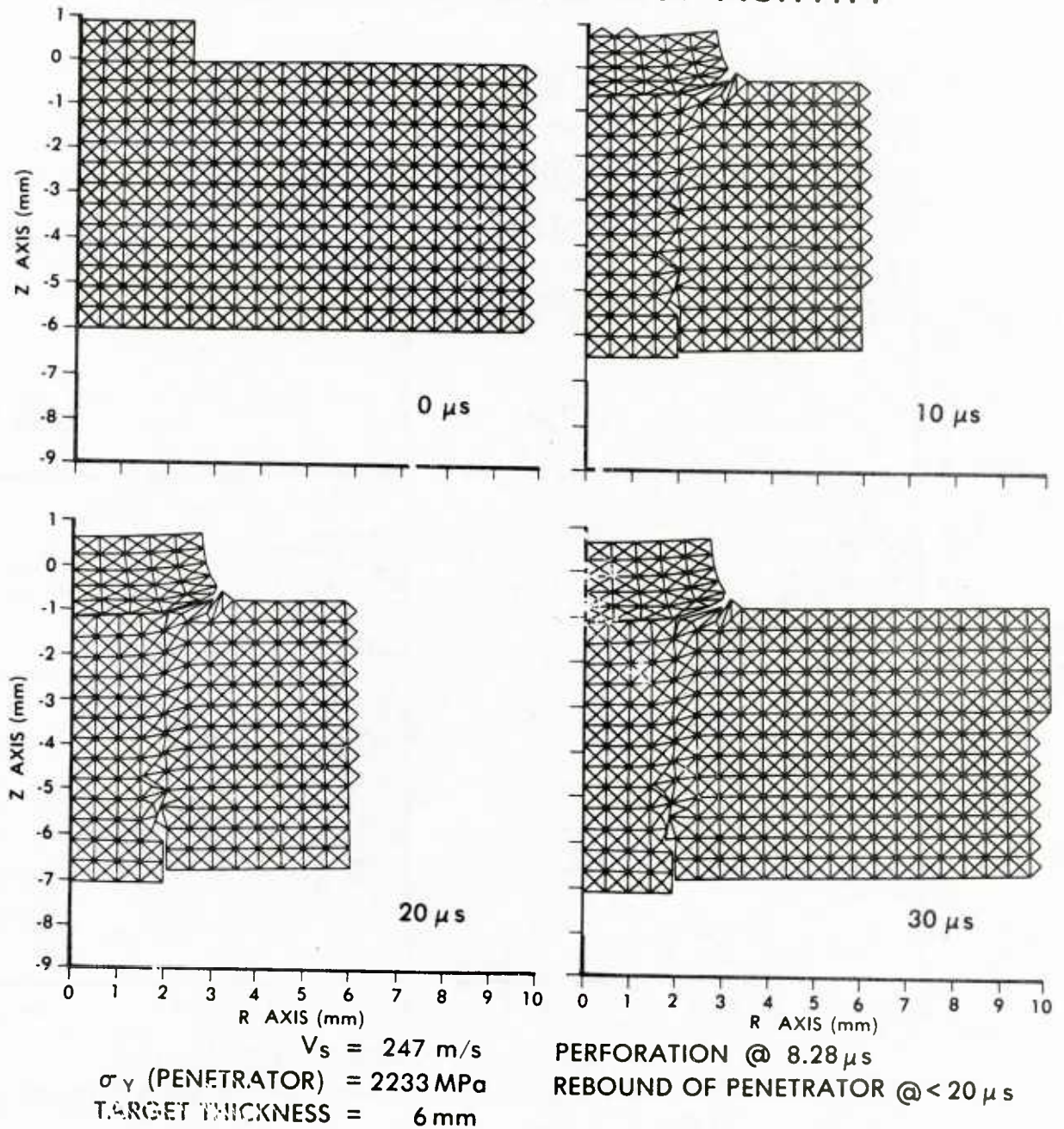
Figure 12a.   Axisymmetric Blowup of Region of Activity - Case II.
100% Plastic Work Converted to Heat.

23

STEEL CYLINDER vs TI 318 TARGET
BLOW UP OF REGION OF ACTIVITY

$V_S = 247$ m/s

σ_Y (PENETRATOR) $= 2233$ MPa

TARGET THICKNESS $= 6$ mm

PERFORATION @ 5.2μs

REBOUND OF PENETRATOR @ $>30 \mu$s
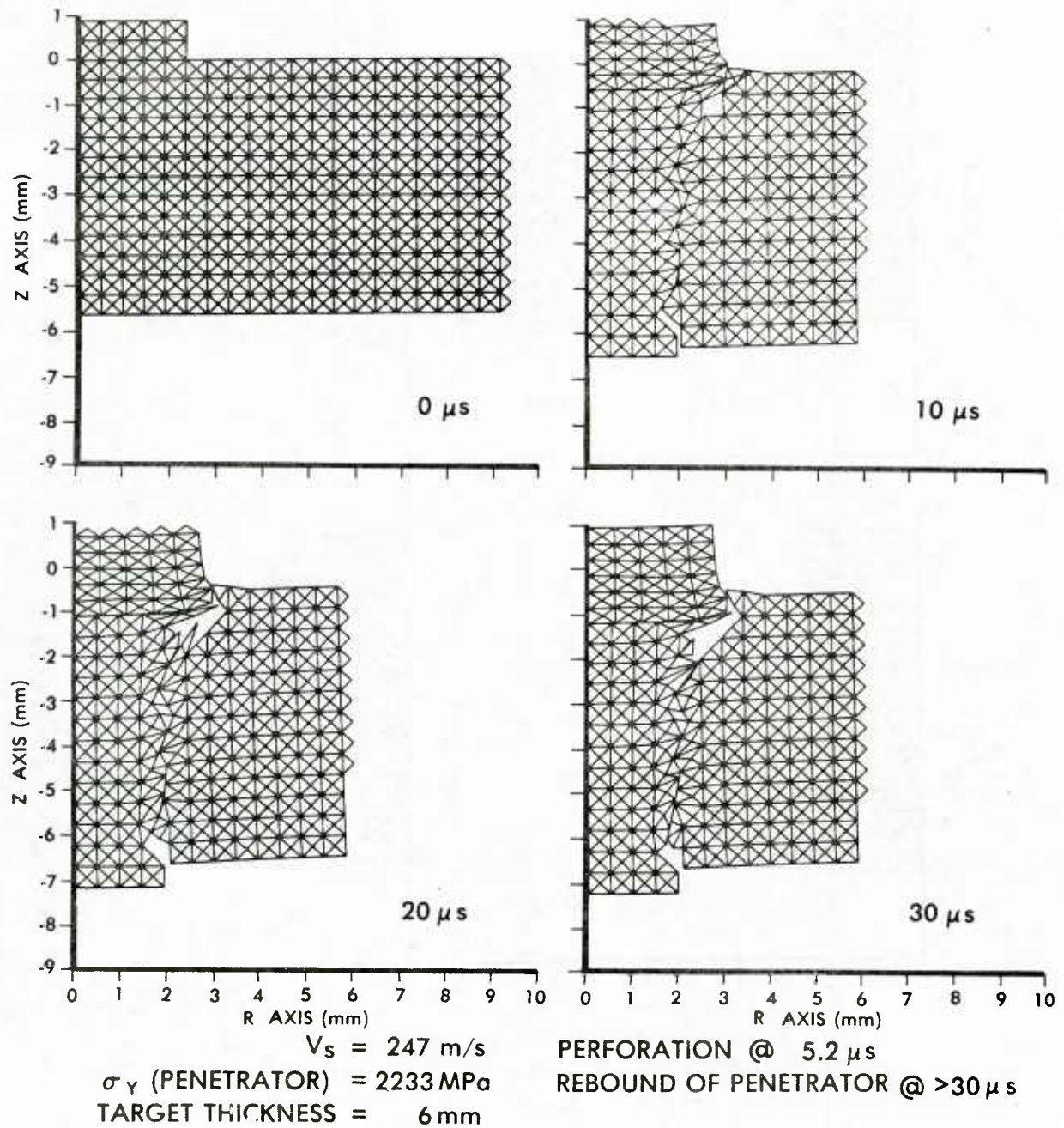
Figure 12b.   Axisymmetric Blowup of Region of Activity - Case II.
85% Plastic Work Converted to Heat.

24
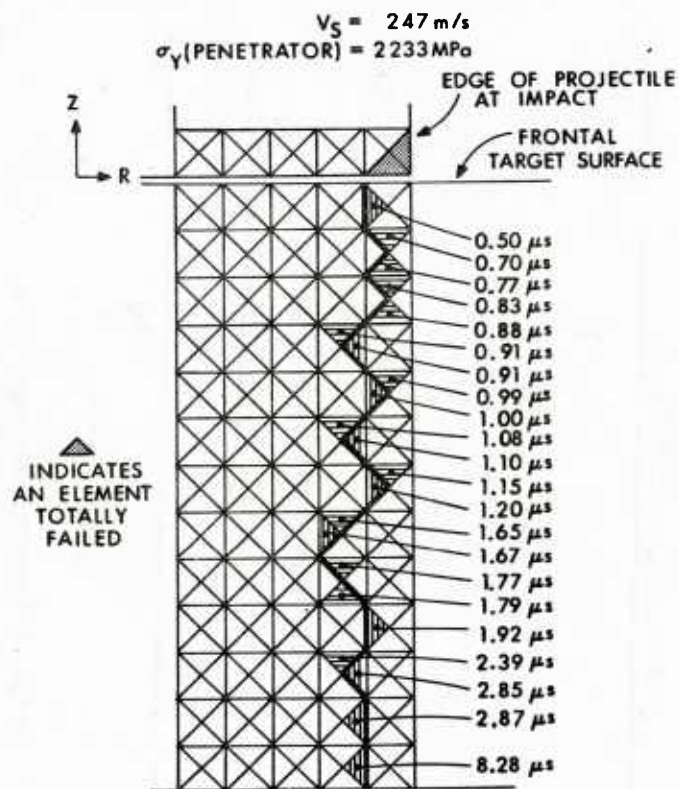
Figure 13a. Pattern of Elements Enabling Split - Case II. 100% Plastic Work Converted to Heat.
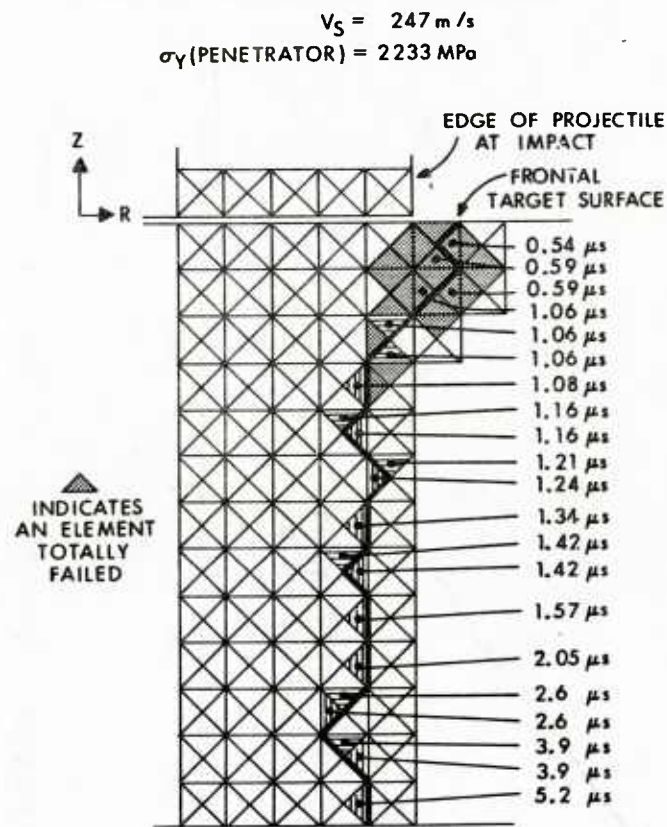
Figure 13b. Pattern of Elements Enabling Split - Case II. 85% Plastic Work Converted to Heat.
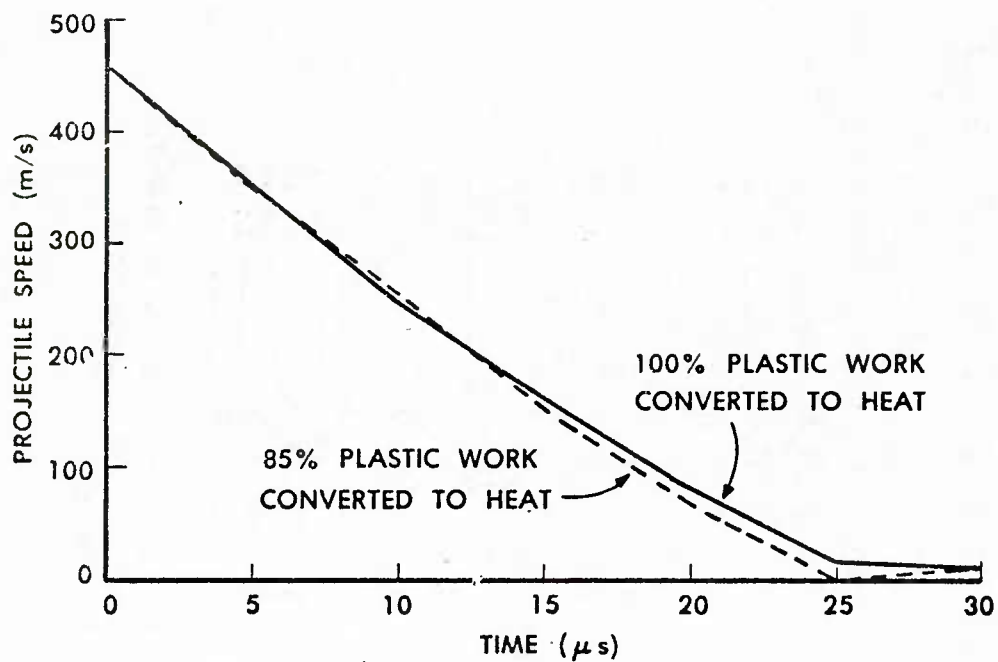
Figure 14. Speed Histories - Case II.
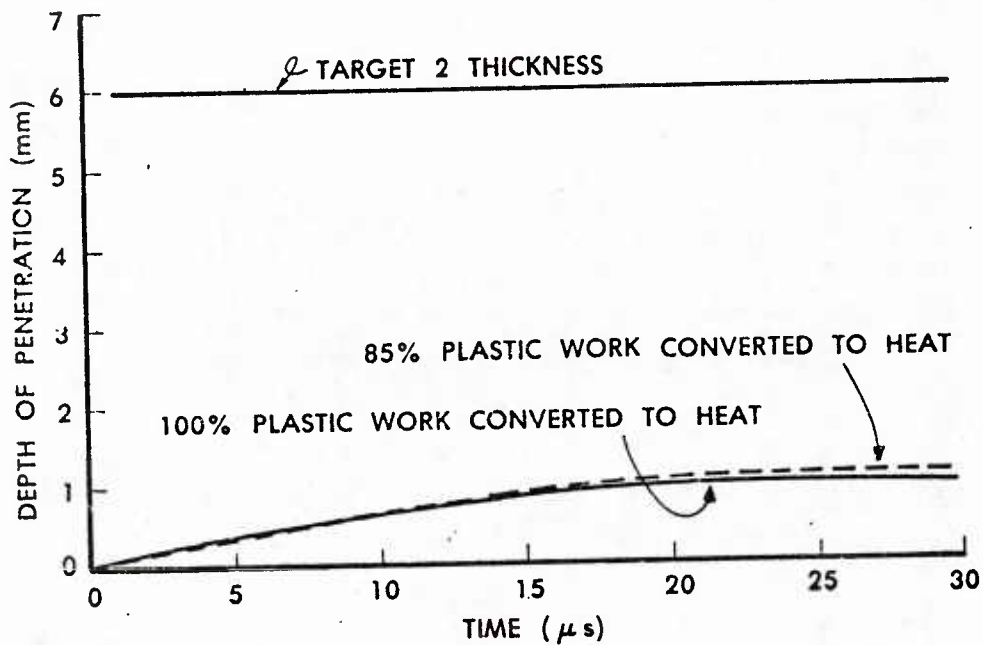
Figure 15. Depth of Penetration Histories - Case II.

and dislodging a plug whereas the lower velocity produced a plug more slowly which remained tightly lodged in the target. There remains a problem in accommodating the plug compression; more accurate material behavior descriptions at high strain rates are required.

It is imperative that criteria which indicate promise in modeling target failure modes be incorporated with available simulation techniques and predictions utilizing such must be tested against experimental evidence. Simulations which can handle only partial penetration of a target or which utilize untested failure criteria can betray penetrator and armor designers. A comparison of the results at 10^{-6}s, splitting disabled, shown in Figures 16 would seem to imply that the Ti318 material is tougher than the Ti125 material when, in truth, experimental results indicate the the Ti318 material is easier to defeat by kinetic energy penetrators. Ti318 has a much higher static strength but its failure mechanism, adiabatic shear, requires far less energy.[16]

The true ballistic worth of these techniques will soon be ascertained when they are applied to impacts involving rolled homogeneous armor and high hard armor. The extrapolation of these techniques to model other target failure situations such as piercing and to model oblique impacts with plane strain simulations is also planned.

----

16. Woodward, R. L., "The Penetration of Metal Targets Which Fail By Adiabatic Shear Plugging," Int. J. Mech. Sci., Vol. 20.
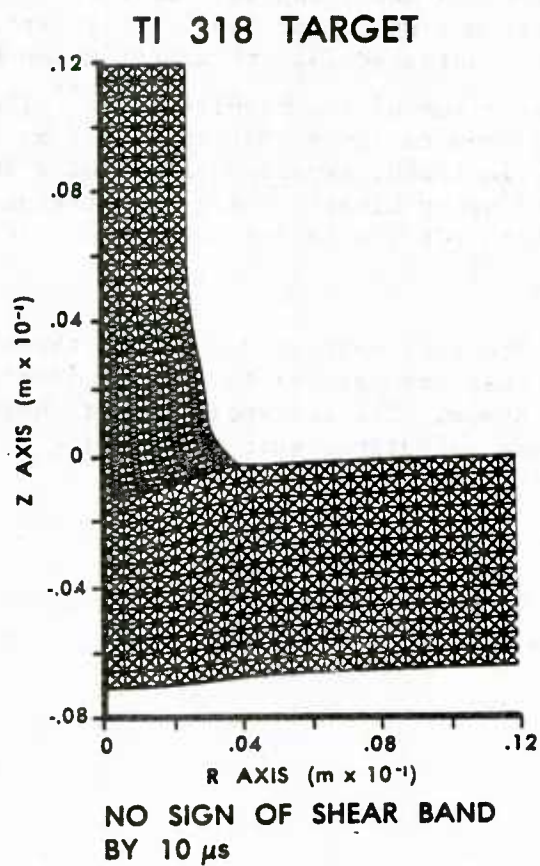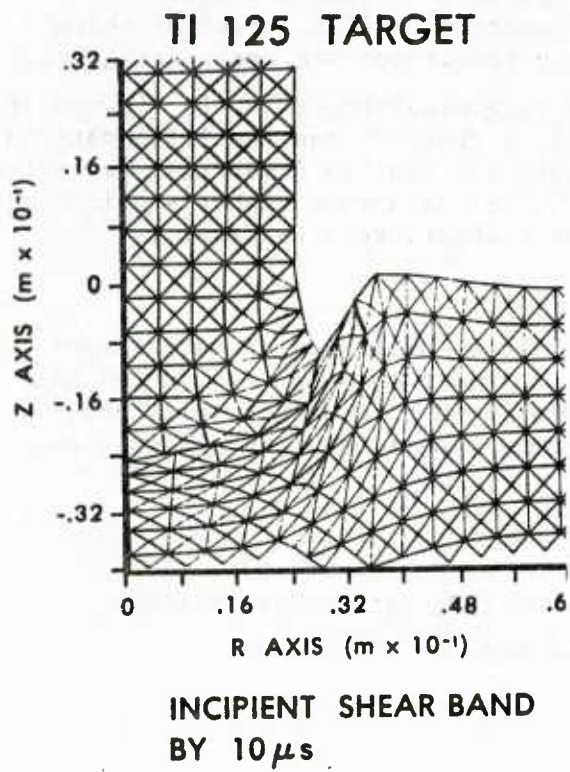
Figure 16. Caution - Simulation Results Can Be Misleading
If Material Failure Not Accurately Modeled.

VII. REFERENCES

1. Johnson, Gordon R., "EPIC-2, A Computer Program for Elastic-Plastic Impact Computations in 2 Dimensions Plus Spin," US Army BRL Contract Report ARBRL-CR-00373, June, 1978. (AD A058 786)

2. Ringers, B. E., "New Sliding Surface Techniques Enable Lagrangian Code to Handle Deep Target Penetration/Perforation Problems," Computational Aspects of Penetration Mechanics, Lecture Notes in Engineering, Springer-Verlag, 1983.

3. Ringers, B. E., "Simulations of Ballistic Impact Situations Involving Deep Penetration and Perforation of Targets with Lagrangian Impact Code," Proceedings of the Army Symposium on Solid Mechanics, 1982 - Critical Mechanics Problems in Systems Design, AMMRC MS 82-4, September 1982.

4. Wulf, G. L., "High Strain Rate Compression of Titanium and Some Titanium Alloys," Int. J. Mech. Sci., Vol. 21, 1979.

5. Recht, R. F., "Catastrophic Thermoplastic Shear," Journal of Applied Mechanics, June, 1964, pp. 189-193.

6. Johnson, Gordon R., Private Communication.

7. Johnson, Gordon R., Hoegfeldt, J. M., Lindholm, US, and Nagy, A., "Response of Various Metals to Large Torsional Strains Over A Large Range of Strain Rates - Part 2; Less Ductile Metals," Journal of Engineering Materials and Technology, January 1983, p. 48.

8. Lindholm, US, "Some Experiments with the Split Hopkinson Pressure Bar," J. Mech. Phys. Solids, Vol. 12, 1964, p. 317.

9. Maiden, C. J., Green, S. J., "Compressive Strain-Rate Tests on Six Selected Materials at Strain Rates From 10^{-3} to 10^{4} In/In/Sec," Transaction of the ASME, September 1966, p. 496.

10. Campbell, J. D. and Ferguson, W. G., "The Temperature and Strain-Rate Dependence of the Shear Strength of Mild Steel," Phil. Mag., Vol. 21, 1970, p. 63.

11. Johnson, W., Impact Strength of Materials, Edward Arnold Ltd., 1972.

12. Rogers, Harry C., "Adiabatic Plastic Deformation," Ann. Rev. Mater. Sci., Vol. 9, 1979, p. 283.

13. Titchener, A. L. and Bever, M. B., Progr. Metal Phys., Vol. 7, 1958.

14. Woodward, R. L., Private Communication - experiments performed at Materials Research Laboratories, Australia.

15. Woodward, R. L., Baxter, B. J. and Scarlett, N. V. Y., "Mechanisms of Adiabatic Shear Plugging Failure in High Strength Aluminum and Titanium Alloys," 3rd International Conference on Mechanical Properties of Materials At High Rates of Strain," Oxford, April 1984.

16. Woodward, R. L., "The Penetration of Metal Targets Which Fail By Adiabatic Shear Plugging," Int. J. Mech. Sci., Vol. 20.

APPENDIX A
## CRITERIA FOR TOTAL ELEMENT FAILURE

All elements were automatically enabled to totally fail under the circumstances discussed below:

1. Minimum time increment violation - A minimum time increment is user assigned, and is based on the time required to travel across the shortest dimension of the triangular element at the sound speed of the material. When a dimension of an element gets too small for the time increment utilized, the choice is to lower the minimum time increment or totally fail the element so that it is no longer processed.

This is a sensitive situation. Lowering the minimum time increment can enable the element to be processed for a longer period of time but it can also allow abnormally high pressures to develop, which, in turn, cause unreasonably high nodal forces and velocities. EPIC-2 checks the kinetic energy; if the kinetic energy of the impact situation increases by more than 10%, a calculation is automatically stopped.

The assumption was made that a reasonable time increment was utilized so the element is totally failed if it violates the minimum time increment. This is the usual reason for totally failing an element.

However, after several elements in an area have totally failed for this reason, there is an adverse effect on nearby elements which results in their total failure due to either -

2. Negative sound speed for an element, implying a severely reduced volume, or

3. Negative area for an element, which results when two nodes reverse position with regard to the third node.

Element failure also requires dynamic relocation of the sliding surfaces. See Appendix B for the details. It is also possible to totally fail elements on an equivalent strain basis, as was done in the original version of EPIC-2. The difference is that master elements are now allowed to fail as well.

APPENDIX B
PROCEDURE FOR HANDLING FAILED ELEMENTS

The procedure for handling a failed element depends on its position with respect to a particular sliding surface; it is a master or slave element on that surface, or neither.

For master and slave elements (m/s elements) the following procedures apply:

1. A m/s element with two consecutive nodes on a m/s surface has its third node inserted in the surface,

2. A m/s element with three consecutive nodes on a m/s surface has its midnode removed from the m/s surface,

3. A m/s element with four consecutive nodes on a m/s surface (the first node is also the last node) has all nodes removed except for the first.

A non m/s element that has failed is kept in reserve and, after another element is totally failed, is checked for m/s status until it becomes a m/s element and is handled above.

A check is also made for duplicated straight line segments which result after some patterns of element failure, i.e. the m/s surface contains node A, node B, and node A again sequentially. In this case, nodes A and B are removed from the m/s surface.

DISTRIBUTION LIST

Copies	Organization	Copies	Organization

1   Commander
Naval Air Development
   Center, Johnsville
Warminster, PA 18974

1   Commander
Pacific Naval Missile Test Center
Point Mugu, CA 93042

12   Administrator
Defense Technical Info Center
ATTN: DTIC-DDA
Cameron Station
Alexandria, VA 22304-6145

1   Commander
David W. Taylor Naval Ship
   Research & Development
   Center
ATTN: Code 1740.4,
      R. A. Gramm
Bethesda, MD 20084

3   Commander
Naval Surface Weapons Center
ATTN: Dr. W. B. Soper
      Mr. N. Rupert
      Code G35,
      D. C. Peterson
Dahlgren, VA 22448

10   Commander
Naval Surface Weapons Center
ATTN: Dr. S. Fishman (2 cys)
      Code R-13,
        F. J. Zerilli
        K. Kim
        F. T. Totan
        M. J. Frankel
      Code U-11, J. R. Renzi
          R. S. Gross
      Code K-22, F. Stecher
        J. M. Etheridge
Silver Spring, MD 20910

1   HQDA
DAMA-ART-M
Washington, DC 20310

9   Commander
Naval Weapons Center
ATTN: Code 31804,
      Mr. M. Smith
      Code 326, Mr. P. Cordle
      Code 3261,
        Mr. T. Zulkoski
        Mr. C. Johnson
ATTN: Code 3181, John Morrow
      Code 3171,
        Mr. B. Galloway
      Code 3831,
        Mr. M. Backman
        Mr. R. F.
          VanDevender, Jr.
      Mr. O. F. R. Heimdahl
China Lake, CA 93555

3   Commander
Naval Research Laboratory
ATTN: Dr. C. Sanday
      Dr. H. Pusey
      Dr. S. Zalesak
Washington, DC 20375

2   Superintendent
Naval Postgraduate School
ATTN: Dir of Lib
      Dr. R. Ball
Monterey, CA 93940

3   Long Beach Naval Shipyard
ATTN: R. Kessler
      T. Fto
      R. Fernandez
Long Beach, CA 90822

1   HQ USAF/SAMI
Washington, DC 20330

1   AFIS/INOT
Washington, DC 20330

1   Commander
US Army Materiel Command
ATTN: AMCDRA-ST
5001 Eisenhower Avenue
Alexandria, VA 22333-0001

Copies	Organization	Copies	Organization
1	ADTC/DLJW (MAJ G. Spitale) Eglin AFB, FL 32542	1	ASD/XRP Wright Patterson AFB, OH 45433
1	ADTC/DLYV (Mr. J. Collins) Eglin AFB, FL 32542	1	HOUSAFE/DOQ APO New York 09012
1	AFATL/DLYB Eglin AFB, FL 32542	1	Director Benet Weapons Laboratory US Army AMCCOM, ARDC
1	AFWL/SUL Kirtland AFB, NM 87117		ATTN: SMCAR-LCB-TL Watervliet, NY 12189
1	Air Force Armament Laboratory ATTN: AFATL/DLODL Eglin AFB, FL 32542-5000	1	Battelle Northwest Laboratories P.O. Box 999 ATTN: G. D. Marr Richland, WA 99352
1	AFATL/DLODR Eglin AFB, FL 32542	4	Lawrence Livermore Laboratory P.O. Box 808
1	AFATL/CC Eglin AFB, FL 32542		ATTN: Dr. R. Werne Dr. J. O. Hallquist Dr. M. L. Wilkins
1	HQ PACAF/OA Hickam AFB, HI 96853		Dr. G. Goudreau Livermore, CA 94550
1	HQ PACAF/DOOQ Hickam AFB, HI 96853	6	Los Alamos Scientific Laboratory P. O. Box 1663
1	HQ TAC/DRA Langley AFB, VA 23665		ATTN: Dr. R. Karpp Dr. J. Dienes Dr. J. Taylor
1	TAC/INAT Langley AFB, VA 23665		Dr. F. Fugelso Dr. D. F. Upham Dr. R. Keyser
1	AUL-LSE 71-249 Maxwell AFB, AL 36112		Los Alamos, NM 87544
1	AFWAL/MLLN (Mr. T. Nicholas) Wright Patterson AFB, OH 45433	6	Sandia Laboratories ATTN: Dr. R. Woodfin Dr. M. Sears Dr. W. Herrmann
1	ASD/FNFSS (S. Johns) Wright Patterson AFB, OH 45433		Dr. L. Bertholf Dr. A. Chabai Dr. C. B. Selleck
1	ASD/FNFFA Wright Patterson AFB, OH 45433		Albuquerque, NM 87115
		1	Commander US Army AMCCOM, ARDC ATTN: SMCAR-TSS Dover, NJ 07801
1	OOALC/MMWMC Hill AFB, HI 96853	1	Commander US Army AMCCOM, ARDC ATTN: SMCAR-TDC Dover, NJ 07801
1	COMIPAC/I-32 Box 38 Camp H. I. Smith, HI 96861		

DISTRIBUTION LIST

Copies	Organization
1	Jet Propulsion Laboratory 4800 Oak Grove Drive ATTN: Dr. Ralph Chen Pasadena, CA 91109
1	Director National Aeronautics and Space Administration Langley Research Center Langley Station Hampton, VA 23365
1	US Geological Survey 2255 N. Gemini Drive ATTN: Dr. Roddy Flagstaff, AZ 86001
1	AAI Corporation P. O. Box 6767 ATTN: R. L. Kachinski Baltimore, MD 21204
1	Aerojet Ordnance Company 9236 East Hall Road Downey, CA 90241

1	Aerospace Research
	  Associates of Princeton,
	  Inc.
	50 Washington Road
	Princeton, NJ 08540

1	Aerospace Corporation 2350 E. El Segundo Blvd. ATTN: Mr. L. Rubin El Segundo, CA 90245
1	AVCO Systems Division 201 Lowell Street ATTN: Dr. Reinecke Wilmington, MA 01887

4	Battelle Columbus Laboratories
	505 King Avenue
	ATTN: Dr. M. F. Kanninen
	    Dr. G. T. Hahn
	    Dr. L. E. Hulbert
	    Dr. S. Sampath
	Columbus, OH 43201

Copies	Organization

4	Boeing Aerospace Company
	ATTN: Mr. G. G. Blaisdell
	    (M.S. 40-25)
	    Dr. N. A. Armstrong,
	    C. J. Artura
	    (M.S. 8C-23)
	    Dr. B. J. Henderson
	    (M.S. 43-12)
	Seattle, WA 98124

2	Brunswick Corporation 4300 Industrial Avenue ATTN: P. S. Chang R. Grover Lincoln, NE 68504
1	Computer Code Consultants, Inc. 1680 Camino Redondo ATTN: Dr. Wally Johnson Los Alamos, NM 87544
1	Dresser Center P. O. Box 1407 ATTN: Dr. M. S. Chawla Houston, TX 77001
1	Effects Technology, Inc. 5383 Hollister Avenue Santa Barbara, CA 93111
1	Electric Power Research Institute P. O. Box 10412 ATTN: Dr. George Sliter Palo Alto, CA 94303

2	Firestone Tire and Rubber
	  Company
	1200 Fireston Parkway
	ATTN: R. L. Woodall
	    L. F. Vescelius
	Akron, OH 44317

1	FMC Corporation Ordnance Engineering Divison San Jose, CA 95114
1	Director US Army TRADOC Systems Analysis Activity ATTN: ATAA-SL White Sands Missile Range, NM 88002

DISTRIBUTION LIST

Copies	Organization	Copies	Organization

1   Ford Aerospace and
Communications Corporation
Ford Road, P. O. Box A
ATTN: L. K. Goodwin
Newport Beach, CA 92663

1   Commander
US Army Communications -
Electronics Command
ATTN: AMSEL-ED
Fort Monmouth, NJ 07703

1   General Dynamics
P. O. Box 2507
ATTN: J. H. Cuadros
Pomona, CA 91766

1   General Electric Company
Lakeside Avenue
ATTN: D. A. Graham, Room 1311
Burlington, VT 05401

1   President
General Research Corporation
ATTN: Lib
McLean, Va 22101

1   Goodyear Aerospace Corporation
1210 Massilon Road
Akron, OH 44315

1   H. P. White Laboratory
3114 Scarboro Road
Street, MD 21154

6   Honeywell, Inc.
Government and Aerospace
Products Divison
ATTN: Mr. J. Blackburn
Dr. G. Johnson
Mr. R. Simpson
Mr. K. H. Doeringsfeld
Dr. D. Vavrick
Dr. C. Candland
600 Second Street, NE
Hopkins, MN 55343

1   Commander
US Army Development and
Employment Agency
ATTN: MODE-TED-SAB
Fort Lewis, WA 98433

1   Northrop Norair
3901 W. Broadway
ATTN: R. L. Ramkumar
Hawthorne, CA 90250

2   Kaman Sciences Corporation
1500 Garden of the Gods Road
ATTN: Dr. P. Snow
Dr. D. Williams
Colorado Springs, CO 80907

1   Lockheed Missiles and Space
Company, Inc.
3251 Hanover Street
ATTN: Org 5230, Bldg. 201
Mr. R. Robertson
Palo Alto, CA 94304

1   Lockheed Missiles and Space
Company, Inc.
P. O. Box 504
ATTN: R. L. Williams
Dept. 81-11, Bldg. 154
Sunnyvale, CA 94086

1   Materials Research Laboratory,
Inc.
One Science Road
Sunnyvale, Ca 94086

2   McDonnell-Douglas
Astronautics Company
5301 Bolsa Avenue
ATTN: Dr. L. B. Greszczuk
Dr. J. Wall
Hungtington Beach, CA 92467

1   New Mexico Institute of
Mining and Technology
ATTN: TERA Group
Socorro, NM 87801

1   Commandant
US Army Infantry School
ATTN: ATSH-CD-CSO-OR
Fort Benning, GA 31905

1   Commander
US Army Tank Automotive Command
ATTN: AMSTA-TSL
Warren, MI 48090

Copies	Organization	Copies	Organization
1	Commander US Army Armament, Munitions and Chemical Command ATTN: SMCAR-ESP-L Rock Island, IL 61299	1	United Technologies Research Center 438 Weir Street ATTN: P. R. Fitzpatrick Glastonbury, CT 06033
2	Orlando Technology, Inc. P.O. Box 855 ATTN: Mr. J. Osborn Mr. D. Matuska Shalimar, FL 32579	1	US Steel Corporation Research Center 125 Jamison Lane Monroeville, PA 15146
1	Systems, Science and Software P.O. Box 1620 ATTN: Dr. R. Sedgwick La Jolla, CA 92038	1	VPI & SU 106C Norris Hall ATTN: Dr. M. P. Kamat Blacksburg, VA 24061
1	Rockwell International Artimetic Missile Systems Div. ATTN: A. R. Glaser 4300 E. Fifth Avenue Columbus, OH 43216	1	Commander US Army Aviation Research and Development Command ATTN: AMSAV-E 4300 Goodfellow Blvd St. Louis, MO 63120
3	Schlumberger Well Services Perforating Center ATTN: J. F. Brooks J. Brookamn Dr. C. Aseltine P. O. Box A Rosharon, TX 77543	1	Westinghouse, Inc. P. O. Box 79 ATTN: J. Y. Fan W. Mifflin, PA 15122
1	Director US Army Air Mobility Research and Development Laboratory Ames Research Center Moffett Field, CA 94035	1	Drexel University Dept. of Mechanical Engr. ATTN: Dr. P. C. Chou 32d and Chestnut Streets Philadelphia, PA 19104
1	Commander US Army Electronics Research and Development Command Technical Support Activity ATTN: DELSD-L Fort Monmouth, NJ 07703-5301	1	Southwest Research Institute ATTN: Dr. C. Anderson 6220 Culebra Road San Antonio, Texas 78228
1	Commander US Army Missile Command ATTN: AMSMI-R Redstone Arsenal, AL 35898	1	Southwest Research Institute Dept. of Mechanical Sciences ATTN: Dr. U. Lindholm 8500 Celebra Road San Antonio, TX 78228
1	Commander US Army Missile Command ATTN: AMSMI-YDL Redstone Arsenal, AL 35898	4	SRI International 333 Ravenswood Avenue ATTN: Dr. L. Seaman Dr. L. Curran Dr. D. Shockey Dr. A. L. Florence Menlo Park, CA 94025

DISTRIBUTION LIST

Copies	Organization	Copies	Organization

2	University of Arizona
	Civil Engineering Department
	ATTN: Dr. D. A. DaDeppo
	         Dr. R. Richard
	Tucson, AZ 85721
		1	West Virginia University
			Dept. of Mechanical and
			   Aerospace Engineering
			ATTN: Dr. N. J. Salamon
			Morgantown, WV 26505

1	University of Arizona
	School of Engineering
	ATTN: Dean R. Gallagher
	Tucson, AZ 85721
		1	University of Oklahoma
			School of Aerospace,
			   Mechanical and Nuclear
			   Engineering
			ATTN: Dr. C. W. Bert
			Norman, OK 73069

1	University of California
	   Los Angeles
	504 Hilgard Avenue
	Los Angeles, CA 90024
		1	University of Dayton
			Impact Physics Research
			   Institute
			ATTN: Dr. S. J. Bless
			300 College Park
			Dayton, Ohio 45469-0001

1	University of California Dept. of Physics ATTN: Dr. Harold Lewis Santa Barbara, CA 93106		

2	University of California
	College of Engineering
	ATTN: Prof. W. Goldsmith
	         Dr. A. G. Evans
	Berkeley, CA 94720
		1	US Army Research and Technology
			   Laboratories
			ATTN: Mr. Wade
			Fort Eustis, VA 23604

2	University of Delaware Dept. of Mechanical Engr. ATTN: Prof. J. Vinson Dr. M. Taya Newark, DE 19711	1	AFATL/DLJW ATTN: 2 LT Michaela Mezo Eglin AFB, FL 32542
1	University of Denver Denver Research Institute ATTN: Mr. R. F. Recht 2390 S. University Blvd. Denver, CO 80210	1	AFATL/DLJW ATTN: 1LT Paul Thee Eglin AFB, FL 32542

1 University of Denver
   Denver Research Institute
   ATTN: Mr. R. F. Recht
   2390 S. University Blvd.
   Denver, CO 80210

ABERDEEN PROVING GROUND

2 University of Florida
   Dept. of Engr. Sciences
   ATTN: Dr. R. L. Sierakowski
            Dr. L. E. Malvern
   Gainesville, FL 32611

    Dir, USAMSAA
      ATTN: AMXSY-D
           AMXSY-MP, H. Cohen
    Cdr, USATECOM
      ATTN: AMSTE-TO-F
    Cdr, CRDC, AMCCOM
      ATTN: SMCCR-RSP-A
           SMCCR-MU
           SMCCR-SPS-IL
    Dir, USACSTA
      ATTN: Mr. S. Keithely

USER EVALUATION SHEET/CHANGE OF ADDRESS

This Laboratory undertakes a continuing effort to improve the quality of the reports it publishes. Your comments/answers to the items/questions below will aid us in our efforts.

1. BRL Report Number_____ Date of Report_____

2. Date Report Received_____

3. Does this report satisfy a need? (Comment on purpose, related project, or other area of interest for which the report will be used.)_____

_____

_____

4. How specifically, is the report being used? (Information source, design data, procedure, source of ideas, etc.)_____

_____

_____

5. Has the information in this report led to any quantitative savings as far as man-hours or dollars saved, operating costs avoided or efficiencies achieved, etc? If so, please elaborate._____

_____

_____

6. General Comments. What do you think should be changed to improve future reports? (Indicate changes to organization, technical content, format, etc.)

_____

_____

_____

	_____
	Name
CURRENT ADDRESS	Organization
	Address
	City, State, Zip

7. If indicating a Change of Address or Address Correction, please provide the New or Correct Address in Block 6 above and the Old or Incorrect address below.

	_____
	Name
OLD ADDRESS	Organization
	Address
	City, State, Zip

(Remove this sheet along the perforation, fold as indicated, staple or tape closed, and mail.)